https://doi.org/10.5194/egusphere-2026-2088
Preprint. Discussion started: 30 June 2026

Novel Possibilities of In-Situ Cloud Observation with Drone-Mountable Holographic Imager

[1]Ari Leskinen, [1]Antonia Radlwimmer*, [1]Uula Isopahkala, [1]Silvia Calderón, [2]David Brus, [2]Konstantinos Doulgeris, [3]Ville Kaikkonen, [3]Eero Molkoselkä, [2,4]Dmitri Moiseev, [4]Marie Lou Hirschy, [3]Anssi Mäkynen, [1]Sami Romakkaniemi and [1]Mika Komppula

[1]Finnish Meteorological Institute, Yliopistonranta 8, FI-70210 Kuopio, Finland

[2]Finnish Meteorological Institute, Erik Palménin aukio 1, FI-00560 Helsinki, Finland

[3]Advanced Electronics Centre, University of Oulu, Pentti Kaiteran katu 1, FI-90570 Oulu, Finland

[4]Institute for Atmospheric and Earth System Research, Faculty of Science, University of Helsinki, Gustaf Hällströmin katu 2, FI-00014 Helsinki, Finland

*Currently at Department of Physics, University of Otago, 362 Leith Street, Dunedin North, Dunedin 9016, New Zealand

Correspondence: Mika.Komppula@fmi.fi

Abstract.

We present a lightweight holographic imaging instrument, the UAV-CPS (Unmanned Aerial Vehicle Cloud Particle Sensor), designed for high-resolution in-cloud particle measurements at a rate of 10 holograms per second. When mounted on a UAV, the instrument samples a well-defined volume of ~3 cm^3 within a single hologram, providing sub-meter spatial resolution within targeted cloud regions such as stratiform cloud tops and cumuliform cloud edges. Compared to conventional platforms, such as research aircraft or tethered balloons, the UAV-based approach offers a cost-effective and versatile alternative, capable of accessing confined or remote areas. This enables improved validation of remote sensing products and provides observational constraints for cloud process rates in numerical cloud models. During a 16-day campaign comprising 14 flights at Pallas, Finland, UAV-CPS measurements were compared against reference instruments installed at the hilltop Sammaltunturi station. On average, UAV-CPS showed lower droplet concentrations in the 5–13 µm diameter range, while larger particles were captured with high accuracy. As with other holographic sensors, detecting and sizing the smallest droplets in a large measurement volume per hologram

https://doi.org/10.5194/egusphere-2026-2088
Preprint. Discussion started: 30 June 2026

remains challenging. However, these limitations are quantified and can be mitigated through calibration, complementary measurements, and ongoing instrument refinement, such as optimizing hologram reconstruction procedures and employing a shorter-wavelength light source. In addition to introducing UAV-CPS, we present a case study that highlights the potential of such instrumentation for high-resolution cloud observations.

1 Introduction

Clouds are a fundamental component of the atmospheric system, exerting a strong influence on large-scale water circulation and atmospheric dynamics (Bony et al., 2015) as well as playing a key role in regulating the Earth's radiative balance. Despite their central importance, clouds remain a major source of uncertainty in climate projections and estimates of climate sensitivity (Cess et al., 1990; Stephens, 2005; Bony et al., 2015: Ceppi et al., 2021; Andersen et al., 2023).

Cloud droplets form when supersaturated water vapor condenses onto aerosol particles and makes them grow from submicron to supermicron sizes. While the fundamental mechanisms, such as aerosol particles acting as cloud condensation nuclei and influencing cloud properties and precipitation, are well established (Twomey, 1977; Albrecht, 1989), the overall impacts of aerosol-cloud-precipitation interactions remain poorly understood. Other concurrent processes may also occur alongside aerosol effects, potentially buffering cloud responses to changes in aerosol properties (Stevens and Feingold, 2009). As a result, even estimates of cloud droplet number concentration susceptibility to aerosol changes remain highly uncertain in both observations and different model applications (Virtanen et al., 2025).

The most challenging questions concern how aerosols affect cloud thickness and lifetime, which are key factors in a cloud’s influence on atmospheric radiative balance. Increased aerosol concentrations lead to an increase in the droplet number, which suppresses droplet growth and delays precipitation formation (Albrecht, 1989, Christensen et al., 2020). Under favorable meteorological conditions, this can enhance cloud liquid water content (LWC) and expand cloud spatial coverage (Christensen et al.,

https://doi.org/10.5194/egusphere-2026-2088
Preprint. Discussion started: 30 June 2026

2024).

On the other hand, cloud droplet number concentration affects the turbulent mixing at cloud boundaries and thus the entrainment of drier air into the cloud. Several studies based on satellite observations and related data retrievals suggest that the increase in droplet concentration in case of nonprecipitating clouds is linked with the reduction in the cloud liquid water path due to more efficient mixing at the cloud top (Gryspeerdt et al., 2019; Possner et al., 2020). This finding is also supported by large eddy simulations which account for the effect of cloud droplet sedimentation and interactions with radiation (Ackerman et al., 2004). More recently, increasing doubt has been presented on the strength of this effect. Satellite-based analyses are subject to retrieval uncertainties and data aggregation related biases (Feingold et al.; 2022, Arola et al., 2022; Kokkola et al., 2025), and co-variability between aerosol loading and meteorological conditions further complicates the interpretation of observed relationships (Goren et al., 2025).

Accurate characterization of small-scale variations in aerosol and cloud particle properties is essential for studying aerosol-cloud-precipitation interactions and related microphysical processes (Kainz and Hoffmann, 2023; Yeom et al., 2024). High-resolution in-situ holographic imaging instruments provide detailed size distributions, number concentrations, and information on particle phase, shape, orientation, and spatial distribution without requiring prior assumptions, in contrast to conventional cloud droplet spectrometers. These capabilities enable retrieval of key cloud properties, including size distribution, number concentration, and thus liquid water content. Recent advances in computational power have further allowed near-real-time operation (Henneberger et al., 2013; Kaikkonen et al., 2020; Zhang et al., 2023). Several research groups have recently employed holographic imaging instruments on a variety of platforms. Ground-based systems enable long-term observations (e.g., Henneberg et al., 2013; Tiitta et al., 2022), while tethered balloons and cable cars facilitate atmospheric profiling (Beck et al., 2017). Equipping aircraft with holographic imagers extends the coverage to larger spatial domains (Desai et al., 2019). More recently, a lightweight imager has been developed for vertical cloud profiling using an untethered weather balloon (Chambers et al., 2023). The main limitation of holographic imaging has been the

https://doi.org/10.5194/egusphere-2026-2088
Preprint. Discussion started: 30 June 2026

maximum resolution, which typically limits the smallest observable droplets to around 6 to 10 µm in diameter. Recently, this has been also extended down to 3.7 µm, which allows better characterization of cloud properties when conditions lead to smaller droplet sizes (e.g. high aerosol loadings in polluted conditions, early stage of cloud lifetime, weak updrafts, high evaporation rates in mixing zones) (Fuchs et al., 2025).

In this study, we demonstrate the feasibility of using the lightweight holographic imaging instrument UAV-CPS, mounted on an uncrewed aerial vehicle (UAV), for in-situ cloud measurements. UAVs are increasingly valuable in atmospheric science, enabling high-resolution sampling of atmospheric properties in environments where manned aircraft or ground-based systems are impractical or cost-prohibitive (Kezoudi et al., 2021). However, conventional instruments are often too heavy or power-intensive for deployment on UAVs with limited payload capacity, highlighting the need for continued development of lightweight, accurate, and energy-efficient in situ probes specifically designed for UAV applications. Such instruments are widely used for meteorological, gas-phase, and aerosol observations; however, relatively few published operational deployments have focused on cloud microphysical properties. Developments beyond conventional optical particle counters toward a highly detailed characterization using holographic imaging systems remain limited (e.g. Kaikkonen et al., 2024; Fuchs et al., 2025). Digital inline holographic imagers offer robust measurement capabilities with light, lensless designs that minimize aerodynamic drag and power consumption.

With the UAV-CPS, the primary objective is to profile cloud interiors and investigate cloud boundaries, particularly cloud tops, to better understand the processes affecting the cloud microphysical properties. UAV-CPS is an enhanced version of the established ICEMET instrument (Kaikkonen et al., 2020; Molkoselkä et al., 2021; Tiitta et al., 2022), featuring a larger open sampling path. When mounted on a UAV platform, it offers greater flexibility in flight path control compared to tethered balloons. During a measurement campaign in Northern Finland, UAV-CPS was deployed alongside other lightweight aerosol and cloud instruments on multiple flights and UAV types, and its performance was also evaluated through comparisons with fixed reference instruments located at ground-based measurement stations. In addition, results from a selected case study were analyzed in the context of prevailing meteorological conditions to better

https://doi.org/10.5194/egusphere-2026-2088
Preprint. Discussion started: 30 June 2026

understand the processes affecting observed droplet size distribution and their vertical variability.

2 Methods

2.1 The flight campaign

The flight campaign took place at the Arctic UAV base of Finnish Meteorological Institute on three days (13, 27, and 29 September 2023). The UAV base is surrounded by a square reserved airspace (area 196 km^2, ceiling 2 km above ground level) as temporary danger (TEMPO D) area named Pallas. The airspace is authorized for beyond visual line-of-sight (BVLOS) operations, and it is centered at the Sammaltunturi station (67.97332N, 24.11572E, 565 m above sea level) that served as a reference point for the vertical profiling during measurement campaigns.

The flight launch site (68.01987N, 24.15016E, 305 m above sea level) was in the middle of an opening with low vegetation enabling smooth launch and landing. Altogether 11 successful flights were selected for the analysis (Tables 1–2). Supporting in situ and remote sensing data on weather, aerosols and cloud properties were gathered from the nearby Sammaltunturi and Kenttärova stations that belong to the Pallas Atmosphere–Ecosystem Supersite (Lohila et al., 2015). Figure 1 illustrates the locations and, as an example of operations, flight paths for flights T2 and V4.

2.2 The UAV fleet

2.2.1 Talon UAV fixed-wing platform

The Talon UAV (X-UAV, Tian–Jie–Li Model Co., Ltd., China) is a fixed-wing airframe that has a wingspan of 1.718 m, a length of 1.1 m, and a maximum take-off weight of about 3 kg. The Talon UAV carried the UAV-CPS and an atmospheric state measurement sensor (Bosch Sensortec BME280) for measuring temperature, relative humidity, and pressure. This platform was chosen because of its flat top, wide fuselage, and adequate mounting surface for the UAV-CPS on the airframe nose (Fig. 2). The data from the flight controller (Matek, H743-WING-V3) and a global positioning system (GPS) were saved on the flight controller's mini-SD card. The UAV-CPS was controlled by a Raspberry pi 4B single board

https://doi.org/10.5194/egusphere-2026-2088
Preprint. Discussion started: 30 June 2026

computer (SBC) from where the holograms were saved on an external 1TB USB3 solid state drive (SSD) with time resolution of 10 Hz and the data from BME280 sensor was saved on a Raspberry Pi Zero with a time resolution of 1 Hz. The take-offs of the Talon UAV were carried out by hand throwing the aircraft (see Fig. 2). The flight was first controlled manually until the aircraft was switched to autopilot mode to follow the programmed flight path (Fig. S1) stored in flight controller's memory. After completing the mission, the flight mode was switched again to manual for belly landing onto a smooth ground.

2.2.2 Vertical take-off and landing uncrewed aircraft system platform

The vertical take-off and landing (VTOL) uncrewed aircraft system (UAS) platform, callsign Marta (Fig. 3), was developed at Finnish Meteorological Institute (FMI) to study aerosol and cloud interactions (ACI) as part of the European Union Aerosol, Clouds and Trace Gases Research Infrastructure (ACTRIS) exploratory platform, mobile platforms (UAV) initiative. The VTOL (Foxtech Ltd., Model Great Shark) frame is made of Kevlar and carbon fiber, and it has a wingspan of 3.2 m and total flight weight of 23 kg. The inner space of about 14 liters is generous for the scientific payload. In this campaign we utilized a pair of condensation particle counters (CPC, TSI Inc. Model 3007) with cut-off diameters of 7 and 15 nm, a portable optical particle spectrometer (POPS, Handix Ltd.) with a measurement size range of 0.15-3 µm, both located inside the VTOL fuselage, and a pair of meteorological sensors (Bosch Sensortec BME280 and Sensirion AG SHT85) outside the VTOL fuselage. The flight location and altitude as well as all data from the sensors were logged on a Raspberry Pi 4 SBC with a resolution of 1 Hz. The aircraft take-offs were controlled manually, and after the transition to fixed-wing mode an autopilot system followed the programmed flight paths stored in the autopilot's memory when in the air. After the mission, the VTOL returned to the launch location and landed autonomously.

2.3 The UAV mounted instruments

Clouds remain a major source of uncertainty in weather and climate models, and process-level understanding requires in situ measurements of droplet number concentration, size distributions, and liquid and ice water content at fine scales.

https://doi.org/10.5194/egusphere-2026-2088
Preprint. Discussion started: 30 June 2026

However, conventional instruments are often too heavy or power-intensive for deployment on small UAVs, where the desired weight would be clearly less than a kilogram with power consumption of less than 20 W to allow reasonable operational times of single missions. For such purposes digital inline holographic imagers offer robust measurement capabilities with lensless designs that minimize aerodynamic drag and energy requirements together with the ability to differentiate between spherical droplets and nonspherical ice particles. These advances promise to significantly enhance the feasibility of high-resolution cloud microphysical data collection, enabling new experiments and expanding observational coverage to under-sampled regions and cloud regimes.

2.3.1 UAV Cloud Particle Sensor

The UAV-CPS (Kaikkonen et al., 2024) is a lightweight (total weight 0.8 kg) digital holographic cloud particle measurement system prototype designed especially to be used on long flights on UAV platforms (power consumption less than 20 W). In our campaign, the UAV-CPS was mounted on the top and front part of the Talon UAV (Fig. 2) with the sampling volume open to the flight direction to ensure undisturbed air flow through the sensor. The sensor operation is based on recording 12 Megapixel resolution digital holograms of cloud particles inside an approximately 3 cm^3 measurement volume with repetition frequency of 10 Hz, resulting in an airspeed-independent sampling rate of 30 cm^3/s. The upper detectable particle size, in turn, is only restricted by the area of the sampling volume, and particles up to millimeter size can be measured.

The recorded holograms were post-processed after each flight. Numerical hologram analysis produced focused shadow images of each individual particle, and the particle sizes and properties were determined from these images. Examples of images are presented in Fig. 4, showing (a) a droplet, (b) a pollen particle, and (c) an ice particle. The particle shapes can be used to distinguish between these types. The particle size distribution was calculated between 5-200 µm, which was divided into typical 1 µm wide size bins.

The performance of the UAV-CPS instrument was characterized more thoroughly than in the initial instrument validation presented by Kaikkonen et al. (2024). The

https://doi.org/10.5194/egusphere-2026-2088
Preprint. Discussion started: 30 June 2026

characterization was based on the same calibration data collected by dispensing a set of NIST-traceable monodisperse glass beads (Whitehouse Scientific, UK). In this study, the non-tracable 5 µm size was left out and data was analysed on the NIST-tracable size range of 9–156 µm. The beads were measured immediately after the field campaign in October 2023.

The beads were blown into the sampling volume using a custom-built manual dispenser. The resulting datasets were analyzed using the same analysis volume definition and filtering criteria as applied in the cloud particle analysis, ensuring consistency between calibration and in-situ measurements.

Particle size metrics (D10, D50, D90) were derived for each bead set, measurement repeatability was analyzed using a block-wise analysis if the data. This provides an estimate of short-term measurement stability, that includes variability from both the instrument and the sampling. Repeatability was expressed as the standard deviation and relative standard deviation (RSD). Combined measurement uncertainty was estimated by combining the repeatability with the uncertainty of the measured reference bead diameters. The number of detected glass beads varied considerably between datapoints, from approximately 10^5 beads for the smallest sizes to on the order of 10^2 particles for the largest sizes. This difference affects the statistical robustness of the derived size metrics, particularly for higher percentiles such as D90.

The purpose of the calibration measurements was to characterize the instrument performance to define parameters for the analysis rather than to apply exact correction factors. It should be noted that glass beads used in the calibration do not have the same optical properties and imaging contrast as water droplets. As results, the uncertainty estimates should be considered indicative and to show a lower bound under high-contrast conditions of the calibration tests. The size-dependent bias, repeatability and combined uncertainty results are presented in Section 3.4. The calibration datasets and analysis scripts are included in the supplementary material.

2.3.2 Condensation particle counters

The two condensation particle counters (CPC model 3007, TSI Inc.) were set to different cut-off diameters, one with 7 nm and the other with 15 nm. With such a configuration,

https://doi.org/10.5194/egusphere-2026-2088
Preprint. Discussion started: 30 June 2026

one can observe freshly nucleated particles in a diameter range of 7-15 nm (e.g. Brus et al, 2021). The CPCs used the same length of the inlet (L=30 cm) made of conductive tubing, led from an additional piece of horizontal stainless-steel main inlet (L=15 cm) going through the VTOL fuselage and facing the flight direction. The inlet was not heated, nor was a dryer used. Due to temperature gradient between ambient and inside the fuselage, most of the in-flight relative humidity fell under 50 %. Penetration for the whole inlet was estimated to be between 90 % and 99 % for particles between 7 and 100 nm and 99 % for particles between 100 nm and 1 µm. The CPC calibration was done in the FMI laboratory through comparison with a Scanning Mobility Particle Sizer (SMPS; model 3938, TSI Inc.) and a CPC (model 3776, TSI Inc.) following the procedures described by Hämeri et al. (2002) and Wiedensohler et al. (2018). The uncertainty of D_{50} values was determined to be ±0.8 nm. The total count of ambient air sample was compared to a full-sized, more precise CPC (model 3772, TSI Corp.) with an agreement of 20 % uncertainty.

2.3.3 Portable optical particle spectrometer

The portable optical particle spectrometer (POPS, Handix Ltd.) is a lightweight instrument for measurements of aerosol number concentrations and size distributions (Gao et al., 2016). It uses a 405 nm diode laser for sizing aerosol particles within the nominal size range of 0.12–4.4 µm in 16 bins based on light scattering from individual particles that are sampled through an inlet nozzle. The POPS was calibrated by the manufacturer and used as such during the whole campaign. However, in-house calibration was done after the campaign, for details see Le at al. (2026). Also, it was reported by several studies (e.g. Pilz et al., 2022; Pohorsky et al., 2024) that the effective lower limit sizing is prone to substantial uncertainties in the first few bins and upper limit for reliable detection is approximately 3 µm. Since caution must be taken when interpreting the lowest and highest size bins. Similarly, as above, the POPS inlet was connected directly to the main inlet with 5 cm of conductive tubing.

2.4 Ground based instruments at Sammaltunturi

We utilized selected continuous aerosol, cloud, and weather measurements at Sammaltunturi station (67.97332N, 24.11572E, 565 m above sea level), which belongs to the Global Atmospheric Watch (GAW) program of World Meteorological Organization

https://doi.org/10.5194/egusphere-2026-2088
Preprint. Discussion started: 30 June 2026

and the Aerosol, Clouds and Trace Gases Research Infrastructure (ACTRIS RI). The station is located on top of a treeless hill, with frequent cloudy conditions, especially during autumns when the visibility drops below 1 km approximately 40 % of the time (Hatakka et al., 2003, Doulgeris et al., 2023). It is approximately 5 km from the flights take-off/landing site.

Cloud interstitial and total aerosol size distributions were measured with a differential mobility analyzer (DMPS) in the size range of 10–800 nm at the time resolution of 6 minutes by utilizing two size-selective sampling inlets: an interstitial inlet with a cut-off of 2.5 µm and a total inlet with no cut-off. The inlets were located at 2 m height above the station's roof and 6 m above the ground, and they were heated to avoid buildup of snow and ice. We estimated the activated particle size distribution and cloud droplet number concentration by integrating the difference between the total and cloud interstitial aerosol size distribution over the measured size range (e.g. Komppula et al., 2005; Virtanen et al., 2025).

Cloud droplet size distribution was measured with two instruments: another holographic imaging instrument, ICEMET (University of Oulu, Finland; Kaikkonen et al., 2020) and a cloud droplet analyzer CDA (Palas GmbH, Germany). The ICEMET was mounted on top of the Sammaltunturi station, approximately 3 m above the rooftop. The operating principle of ICEMET is the same as that of the UAV-CPS, although it has a smaller sampling volume of approximately 0.3 cm^3. The instrument has a wind vane to turn it so that the sampling volume is open to the prevailing wind. The ICEMET measurements were carried out at the time resolution of two seconds, and the analyzed size range of 5–200 µm. The CDA is an optical aerosol spectrometer designed to measure the size distribution and number concentration of aerosols and cloud droplets. It operates on the principle of Mie scattering, detecting individual particles within an optically defined measurement volume. The CDA covers a size range from approximately 0.4 to 94 µm (in water-equivalent diameters). The CDA is configured with a Sigma inlet and a vertically oriented sampling system. It is important to note that the combination of the Sigma inlet and vertical orientation may lead to some cloud droplet losses. Further details on the instrument setup, calibration, and possible losses can be found in Doulgeris et al. (2025). The CDA measurements were carried out with a time resolution of 10 seconds and

https://doi.org/10.5194/egusphere-2026-2088
Preprint. Discussion started: 30 June 2026

averaged over one minute time intervals for further analysis.

2.5 Cloudnet instruments at Kenttärova

The Kenttärova station (67.98732N, 24.24326E, 347 m above sea level) is located at the foot of the Sammaltunturi hill. Established in 2002 and featuring a 20-meter-high measurement tower, the station provides data for studying atmosphere–biosphere interactions above a spruce forest (Lohila et al. 2015). In 2023, the station was equipped with cloud remote sensing measurements, and the station provides data from a Doppler cloud radar (model RPG-FMCW-94 RPG Radiometer Physics GmbH), ceilometers (Vaisala CL31 and CL61), a HALO Doppler wind lidar (HALO Photonics) and meteorological instruments, for details see Tukiainen et al., (2025). These data are processed and curated at the ACTRIS Cloudnet data portal that produces several daily data products.

In this work, the variable 'target classification' in the Classification product (O'Connor, 2024a; O'Connor, 2024b; O'Connor, 2024c) was used to characterize the cloud status at each altitude during the flights. It must be noted that the distance between the flight route and Kenttärova station was approximately 5 km, so the cloud on the flight route may not have been identical to that classified by the Cloudnet.

2.6 Derived cloud properties

We calculated the LWC as the sum of the masses of individual cloud droplets within the sampling volume, assuming a unit density of liquid water (1000 kg m^{-3}). LWC reflects the bulk amount of condensed water in the measured air parcel. The median volume diameter (MVD) was defined as the droplet diameter at which half of the total liquid water volume is contained in smaller droplets and half in larger ones. While LWC provides information on the absolute amount of liquid water, MVD is a robust measure of the characteristic droplet size within the distribution

2.7 Cloud model simulations

To better understand the dynamics of the observed cloud and support the data analysis, we performed Large-Eddy-Simulations (LES) for the selected cloud case of 27 September 2023, a double-layer cloud system comprising our sampling target a low-level liquid

https://doi.org/10.5194/egusphere-2026-2088
Preprint. Discussion started: 30 June 2026

stratocumulus cloud laying below a high-altitude ice cloud. Our research aimed to examine how boundary layer dynamics could have been affected by overlying ice clouds and by changes in the extent of coupling with surface-generated turbulence. We worked with UCLALES-SALSA, a state-of-the-art model that accounts for aerosol-cloud-turbulence-radiation interactions combing the LES modelling framework of UCLALES (University of California Los Angeles large-eddy simulation model, Stevens et al., 2005) with the cloud microphysical scheme of SALSA (Sectional Aerosol representation module for LArge-Scale Applications, Tonttila et al., 2017; Tonttila et al., 2021). With a sectional dry-aerosol representation, the model simulates the transition from aerosols to cloud droplets, raindrops, and ice particles without prescribed size distributions or parameterized process rates. The UCLALES-SALSA has been previously used to simulate similar low altitude clouds producing high degree of closure with observations (Calderón et al., 2022).

The model was initialized using vertical profiles of atmospheric variables derived from the ECMWF-ERA5 reanalyzed hourly data for a spatial area of 0.5 degrees x 0.5 degrees in latitude and longitude centered around the flight launch site. (Hersbach et al., 2023). Small adjustments for the boundary layer temperature and moisture content were made to adjust the cloud base at observed altitude. The model domain spanned 49 km^2 in area and 1.5 km in height, with horizontal and vertical resolutions of 50 m and 10 m, respectively. Additional details on model initialization can be found in the supplemental information.

3 Results

3.1 Overview

The exact times and maximum altitudes for each flight, as well as the cloud top altitude, are given in Tables 1–2. Figure 5, in turn, illustrates the respective target classification plots from the Cloudnet, zoomed to 0.4–3 km range. For a wider view of the cloud layers also at higher altitudes up to 12 km, the radar reflectivity factor products for each day are shown in Supplement (Fig. S2). The bars on top of the classification product plots in Fig. 5 show the relative timing of the flights with different aircraft as an indication of

https://doi.org/10.5194/egusphere-2026-2088
Preprint. Discussion started: 30 June 2026

comparability of different measurement instruments with respect to the cloud structure. The UAV-CPS sampled the first cloud once on 13 September. The second and third clouds were each revisited three times on 27 and 29 September, respectively, enabling three successive observations of cloud evolution within approximately three hours (27 September) and two hours (29 September). Although seven successful flights were performed, in the following we will mainly concentrate on the flights T3 and T4, as those provided continuous cloud deck. During T4, also the cloud base was low enough for reference observations at the Sammaltunturi ground station. The cloud particle measurement uncertainty of the UAV-CPS is assessed in Section 3.4 and is used to support the following comparisons.

3.2 UAV-CPS intercomparison with surface-based instrumentation

Figure 6 shows particle size distributions between 400 and 1200 m above sea level during flight T4, using the UAV-CPS. Data were averaged over 100 m altitude intervals. Although the instrument analyzed particles within the 5–1000 µm size range, 99.96 % of the particles were smaller than 50 µm, and thus the size axis in Fig. 6 was limited to 5–50 µm for clarity.

Close to the cloud base, the observed droplet size distribution was unimodal, with a median number diameter of 9.8 µm. This mode grew with a median diameter increasing with height reaching a median diameter of 24.1 µm at the cloud top, while the number concentration within the mode decreased, particularly during ascent period of flight. At the cloud top, a second mode emerged, dominating the total droplet concentration. This bimodal feature was observed during both ascent and descent although the differences between those observational periods highlighted the variability in the cloud properties, especially in the upper half of the cloud (Figure 7).

Figure 8 compares droplet size distribution measured by UAV-CPS at 550–580 m altitude with concurrent ICEMET and CDA measurements at Sammaltunturi. All three instruments showed the peak concentration at almost the same size: The derived MVDs were 12.5 µm (UAV-CPS), 12.1 µm (ICEMET), and 9.0 µm (CDA). Concentrations from

https://doi.org/10.5194/egusphere-2026-2088
Preprint. Discussion started: 30 June 2026

UAV-CPS and ICEMET matched closely for droplets greater than 13 µm, while below 13 µm UAV-CPS underestimated particle concentrations by 24-100% relative to ICEMET. Differences at the larger end of the size spectrum were also observed, likely due to spatial separation of the instruments and inhomogeneity in cloud structure, which is analyzed in more detail in the following section.

The lower size ranges from ICEMET and CDA at Sammaltunturi agreed well, indicating good agreement between those instruments. Direct comparisons, however, remain challenging due to differences in calibration procedures: while particle size was calibrated, number concentration was not.

Based on DMPS analysis, the estimated concentration of activated particles was 183 cm^{-3}. Measured average CDNCs were 192 cm^{-3} for ICEMET and 94 cm^{-3} for CDA (Fig. 7). For UAV-CPS, average CDNC at Sammaltunturi height was 112 cm^{-3} during ascent and 124 cm^{-3} during descent, peaking at 145 cm^{-3} during the latter. Differences between ascent and descent periods indicate variability in cloud structure and even the cloud top height during flight T4. Figure S3 provides similar comparisons to Figure 7 for all UAV-CPS flights (T1-T7).

Overall, DMPS analysis and ICEMET agreed well, whereas UAV-CPS and CDA reported concentrations about 40–50% lower. In case of the CDA, the discrepancy likely stems from the particle losses in the CDA inlet (Doulgeris et al., 2026 to be submitted). In case of UAV-CPS, the reduced sensitivity to the smallest particles is likely to contribute, but also the spatial difference between the Sammaltunturi station and the flight paths might cause uncertainty. These differences naturally impact the derived LWC, which was 0.145 g/m^3 (UAV-CPS), 0.199 g/m^3 (ICEMET), and 0.028 g/m^3 (CDA).

3.3 Case study on aerosol cloud interactions

Next, we utilized the UAV-CPS, POPS, and CPC measurements to examine aerosol-cloud processes during a warm cloud case observed on 27 September 2023 between 14:19 and 16:05 UTC. The analysis focuses on data collected during VTOL flight V4 and Talon UAV flight T3. According to the Cloudnet target classification product (Fig. 5), the observed cloud extended from about 500 m to 1300 m altitude above sea level. The temperature within the cloud ranged from 8.0 °C at cloud base to 5.0 °C at cloud top (Fig. 9). The

https://doi.org/10.5194/egusphere-2026-2088
Preprint. Discussion started: 30 June 2026

temperature inversion at and above the cloud top was weak. During the different VTOL penetrations, it varied between 0.1 and 1.7 °C, being on average 0.6 °C, which is much less than typically in the marine stratocumulus clouds for example.

Figure 9 shows the vertical profiles of aerosol and cloud properties from the two flights as a combined case study. In this case, the total aerosol concentration just below the cloud base was 680 cm^{-3}. At cloud base (~500m), droplet activation reduced the aerosol concentration to an average of 322 cm^{-3}, suggesting that approximately 53 % of particles were activated into cloud droplets when a well-mixed boundary layer is assumed. The decrease in concentration was strongest for >150 nm particles, of which 72 % were scavenged. Within the cloud, aerosol concentration gradually increased with altitude, reaching 520 cm^{-3} at the altitude of 1040 m. Above this level, the aerosol concentration rose sharply to 1041 cm^{-3} at the cloud top (1270 m). This increase in concentration was strongest for aerosol particles between 7 and 150 nm in diameter. At the cloud top, also the concentration of 7–15 nm particles increased, indicating the existence of freshly nucleated aerosol particles (Keil and Wendish 2001).

Within the cloud, a fraction of accumulation mode particles was activated into cloud droplets (cloud scavenging), and these droplets grew with altitude (Fig. 9), in a similar way as during flight T4 (Fig. 6). Again, the highest cloud droplet number concentration values were observed at the cloud base and near the cloud top. The presence of a high number of relatively small droplets in these layers indicates that activation is taking place in both layers. These particles grew quickly to sizes of approximately 10 µm in diameter. At the cloud top, these small droplets coexisted with larger ones, resulting in a bimodal droplet size distribution, as seen in flight T4 (Fig. 6).

Above the inspected cloud, a second cloud layer was observed at an altitude of 4-8 km (Fig. S2). This upper cloud layer suppressed radiative cooling, thereby suppressing turbulence formation in the boundary layer, a process that typically occurs in the absence of such a second layer (Leung et al., 2016). Since surface sensible heat flux was also very low as inspected from the ERA5 reanalysis, the boundary layer was likely decoupled. As a result, the number of cloud droplets could be smaller than estimated based on surface aerosol measurements alone. To explore this further, we performed

https://doi.org/10.5194/egusphere-2026-2088
Preprint. Discussion started: 30 June 2026

large eddy simulations. The results confirmed a decoupled boundary layer, with a minimum updraft velocity near 400–450 m, closely corresponding to the cloud base (Fig. S5a). At this altitude the characteristic updraft velocity was simulated to be ~0.13-0.15 m/s. Under these decoupled conditions, the simulation showed that the reduction of CCN particles, with sizes larger than 80nm in diameter, within the cloud layer was much faster than in the surface-connected layer (Fig S5c). Specifically, CCN concentrations in the cloudy layer decreased by approximately 4.7 % per hour, whereas the loss rate in the surface-connected layer was less than 1 % per hour. Over time, this mechanism could lead to aerosol profiles consistent with observations.

Interestingly, elevated concentrations of relatively small cloud droplets were observed near the cloud top. Due to the weak inversion, which was several degrees per kilometer less than is typical, for example, in marine stratocumulus, it is possible that free-tropospheric air entrained into the cloud layer, leading to the activation of new cloud droplets at the cloud top. In the case of low radiative cooling, this process might have been triggered by local topography, as the fells surrounding the observation area rise to 300 m above the local lake level with slopes up to 24 degrees. An alternative explanation for the small-droplet mode is heterogeneous evaporation within a diluting air parcel lifted through the inversion by stronger updrafts from the boundary layer. However, given the current setup of instrumentation in the two different UAV's, it is difficult to conclude which was the dominant mechanism. Orography may also have affected the surface-based droplet measurements, which had higher droplet concentrations than those from the airborne instruments. In the case of a decoupled boundary layer, hill slopes could introduce higher amounts of aerosol into the cloud layer from the surface. This, together with the increased updraft caused by the hill slope, could contribute to the higher concentration of small cloud droplets seen in Figure 8 (Anttila et al., 2012, Romakkaniemi et al., 2017). As illustrated in the topography map (Fig. S1), Sammaltunturi station is susceptible to such effects from all wind directions. These processes naturally increase the uncertainty when comparing surface- and airborne-based droplet size distributions, particularly for smaller droplets, which adjust rapidly to changes in environmental conditions.

It should be noted that the UAV-CPS flight occurred approximately 80 minutes after the

https://doi.org/10.5194/egusphere-2026-2088
Preprint. Discussion started: 30 June 2026

Aerosol-VTOL flight, which may explain some of the differences as the cloud processes could slowly decrease the aerosol and thus cloud droplet concentration. However, Cloudnet profiles did not indicate significant change in the classification of the lower cloud during these flights, as both featured drizzle and droplets. Only shortly after the latter flight, Cloudnet indicated that rain initiated from the cloud above.

3.4 UAV-CPS measurement uncertainty and calibration performance

The results of the performance characterization and uncertainty analysis of the UAV-CPS are shown in Fig. 11 and Fig. 12. The calibration analysis revealed a clear size-dependent measurement performance of the instrument, as typical for holographic instruments. The block-wise analysis resulted in a relative standard deviation (RSD) of approximately 1–3% for D50 across the particle size range investigated, which indicates stable short-term measurement performance. Repeatability remained below 2% for most particle sizes and did not show strong dependence on particle diameter.

Systematic bias was found to have a typical behavior for holographic imaging systems, the sizes close to the optical resolving power are overestimated. In the case of UAV-CPS, the smallest bead size (~9 µm) was overestimated by approximately 10–15%, whereas the largest bead sizes had very small relative bias.

The combined expanded uncertainty (k = 2), which includes both repeatability and reference measurement uncertainty, increased with particle size. This reflects both the increasing spread in the measurement results and the uncertainty of the reference bead diameters, which exhibit quite large size range. In relative terms, the measurement uncertainty remained low across the whole investigated size range.

Overall, the results indicate that random measurement variability remains small compared to the systematic effects, especially for small particle sizes. Consequently, the differences observed in the in-situ measurements between UAV-CPS and other instruments in Section 3.2 primarily result from the size-dependent detection efficiency and resolution limitations which affect the detection of the smallest cloud particles.

4 Discussion

https://doi.org/10.5194/egusphere-2026-2088
Preprint. Discussion started: 30 June 2026

The newly developed lightweight holographic imaging sensor, UAV-CPS (Kaikkonen et al., 2024), demonstrated reliable performance when mounted on a fixed-wing UAV, enabling high-frequency in-situ cloud particle measurements. Detailed comparisons between UAV-CPS and the reference sensor ICEMET revealed some expected limitations, particularly in detecting the smallest particles.

The theoretical lateral optical resolution of the UAV-CPS varies inside the measurement volume between approximately from 5 µm to 10 µm. This means that the size of the smallest particles can be determined accurately only inside the volume of the higher optical resolution, which is situated on the camera side of the measurement volume. This variation in optical resolution also leads to the non-detection of some of the smallest particles (< 10 µm), as the intensity of their shadow images decreases with distance from the detector and may fall below the detection threshold of the hologram analysis algorithm. This is analogous with our results, which showed that UAV-CPS likely underestimated the number concentration of particles smaller than 10 µm in diameter compared with ICEMET (Fig. 8). This discrepancy is partly due the varying optical resolution of the UAV-CPS across the measurement volume, in contrast to ICEMET's more uniform optical resolution of 5 µm or better. Holographic systems are also known to overestimate particle sizes near their lateral optical resolution limit (Henneberger et al., 2013; Kaikkonen et al., 2024). For example, UAV-CPS measured a median diameter of 8.4 µm for monodisperse 5 µm glass spheres (Kaikkonen et al., 2024), illustrating resolution-related detection uncertainty. Consistently, the calibration results presented here show a clear size-dependent bias for particles below approximately 10 µm in diameter. In the future, the accuracy of concentration and particle-size measurements for particles smaller than 10 µm in the UAV-CPS could be improved by developing analysis scripts that restrict the analysis volume to the higher-resolution regions specifically used for detecting these smallest particles. Such an analysis script would very likely also enable the application of a calibration correction factor to determine the smaller particle sizes more accurately, which is currently not feasible for the UAV-CPS, unlike in the case of the ICEMET. Without such calibration, resolution limitations can lead to considerable uncertainties in derived parameters such as LWC, especially close to the cloud base where average droplet size is small. In addition, if a suitable shorter

https://doi.org/10.5194/egusphere-2026-2088
Preprint. Discussion started: 30 June 2026

wavelength laser diode can be found for the UAV-CPS, it would improve the achievable theoretical optical resolution and enable the detection of smaller droplets in a larger volume than is currently possible. In summary, future investigations should assess how the proposed approaches for limiting the measurement volume in all three dimensions could improve small-particle detection, and whether changes in the optical configuration—such as employing a shorter-wavelength laser diode—could further enhance resolution and particle segmentation.

Derived quantities such as MVD and LWC are sensitive not only to the accurate determination of droplet sizes but also to the calibration of number concentration measurements. Many cloud instruments lack proper calibration of particle number concentrations, which can introduce significant uncertainties in LWC estimates. In contrast, holographic imaging instruments generally provide reliable number concentration measurements, as the sampling volume is well-defined, and the number of droplets within this volume can be accurately counted. This advantage contributes to improved confidence in LWC retrievals despite remaining challenges related to size resolution.

Parallel measurements using complementary instruments, such as POPS for aerosol characterization and a miniaturized cloud droplet probe, would help to mitigate limitations related to size resolution and sampling volume. Although such measurements were not conducted here on a single platform, the combined use of POPS and UAV-CPS has strong potential to provide detailed insights into aerosol–cloud interactions. So far simultaneous observations have often relied on coordinated operation of multiple UAVs, which introduces additional spatiotemporal uncertainty in the intercomparison of measured size resolution and sampling volume. This is changing with smaller instruments and the employment of larger UAVs.

An alternative approach would be to perform simultaneous measurements using multiple instruments mounted on a tethered balloon, which typically provides a substantially higher payload capacity than most uncrewed aerial vehicles (UAVs). This configuration would enable concurrent observations within the same cloud volume (Schlenczek et al., 2025). The more appropriate platform ultimately depends on the

https://doi.org/10.5194/egusphere-2026-2088
Preprint. Discussion started: 30 June 2026

specific application and operational environment. While tethered balloons offer increased payload capacity and longer sampling durations, their maneuverability is limited, and they impose operational constraints, particularly in environments with obstacles such as trees, masts, or power lines.

UAV mounted lightweight instruments have also potential for verifying and improving remote sensing measurements, such as the Cloudnet products. As an example, Figure 12 compares the vertical profiles of effective diameter, and liquid water content calculated from the UAV-CPS data from Cloudnet and Sammaltunturi station measurements. The differences can be attributed not only to limitations in UAV CPS sizing but also to uncertainties in the retrieval of cloud microphysical properties from remote sensing observations, as well as to spatial separation since the flight routes were located approximately 5 km from the Cloudnet site. A more detailed analysis is needed to quantify the impacts of the retrieval and collocation uncertainties.

5 Conclusions

This study demonstrates that the lightweight holographic imaging sensor UAV-CPS, when mounted on a UAV platform, provides high-resolution cloud particle measurements at high temporal resolution. The portability and operational flexibility of the system allow targeted in situ observations in specific cloud regions, such as stratiform cloud tops and cumuliform cloud edges.

Compared to traditional platforms like research aircraft or tethered balloons, the UAV-based system offers a cost-effective and flexible alternative, with the added benefit of being deployable in more confined or remote locations. This capability opens new possibilities for highly targeted observations, for example improving products from cloud radars in a location like Pallas, where it is possible to fly directly above the instrument. Moreover, UAV measurements can support the validation of satellite remote sensing products, where retrieved properties, such as cloud droplet effective radius, are sensitive to variability in cloud microphysical properties (Kokkola et al., 2025). Finally, these high-resolution in situ observations can enhance cloud process models, facilitating the connection between microphysical measurements and cloud dynamics

https://doi.org/10.5194/egusphere-2026-2088
Preprint. Discussion started: 30 June 2026

(Calderón et al., 2022).

Although the sensors' uncertainty in sizing the droplets in a range of 5-10 is higher than for larger droplets, this is well-characterized and can be addressed through calibration, complementary measurements, and future instrument development. Improving optical resolution, for example, by optimizing the measurement volume and using a shorter-wavelength light source may further enhance the accuracy of small-particle detection. The successful use of UAV-CPS in combination with aerosol observations in this study highlights the value of multi-instrument approaches for capturing a wider size and concentration spectrum.

The development of miniaturized sensors such as UAV-CPS represents a significant step forward in enabling cloud microphysical measurements. When operated from UAVs, these instruments allow sub-meter scale resolution of cloud properties at the cloud top, which remains a critical region in reducing uncertainties in the modelling tools used for climate projections.

Data availability. The Cloudnet data used in this study are generated by the Aerosol, Clouds and Trace Gases Research Infrastructure (ACTRIS) and are available from the ACTRIS Data Centre using the links given in the references. Other data is stored in Finnish Meteorological Institute's research data repository METIS (10.57707/fmi-b2share.fadgq-2fd93).

Author contributions. AL, AM, SR, and MK led the different parts of the research projects involved. DB, KD, VK, and EM carried out campaign planning, instrument calibration, flight operations and in-situ measurements. AL, AR, and UI developed measurement data processing codes. SC and SR performed the simulations. AL was responsible for preparing the manuscript with contributions from all co-authors. All authors reviewed and edited the manuscript, provided critical feedback, and helped shape the research and analysis.

Competing interests. The authors declare that they have no conflict of interest.

Acknowledgements. We acknowledge ACTRIS and Finnish Meteorological Institute for

https://doi.org/10.5194/egusphere-2026-2088
Preprint. Discussion started: 30 June 2026

providing the data set which is available for download from https://cloudnet.fmi.fi. We acknowledge ECMWF for providing IFS model data.

Financial support. The authors gratefully acknowledge tie financial support of the Research Council of Finland for the projects: SHARPCLOUD (decisions no. 347968 and 348080) and 4Dcloud (decisions no. 369600 and 369601), and the Jane and Aatos Erkko Foundation for PERHO project (grant no. 210047).

References

Ackerman, A. S., Kirkpatrick, M. P., Stevens, D. E., and Toon, O. B.: The impact of humidity above stratiform clouds on indirect aerosol climate forcing, Nature, 432, 1014–1017, https://doi.org/10.1038/nature03174, 2004.

Albrecht, B.A.: Aerosols, cloud microphysics and fractional cloudiness, Science, 245, 1227–1230, 1989.

Andersen, J. K., Stier, P., Sato, Y., Myhre, G., and Mülmenstädt, J.: Cloud adjustments dominate the overall uncertainty in the global warming response to carbon dioxide, *Atmos. Chem. Phys.*, 23, 10775–10791, https://doi.org/10.5194/acp-23-10775-2023, 2023.

Anttila, T., Brus, D., Jaatinen, A., Hyvärinen, A.-P., Kivekäs, N., Romakkaniemi, S., Komppula, M., and Lihavainen, H.: Relationships between particles, cloud condensation nuclei and cloud droplet activation during the third Pallas Cloud Experiment, Atmos. Chem. Phys., 12, 11435–11450, https://doi.org/10.5194/acp-12-11435-2012, 2012.

Arola, A., Lipponen, A., Kolmonen, P., Virtanen, T. H., Bellouin, N., Grosvenor, D. P., Gryspeerdt, E., Quaas, J., and Kokkola, H.: Aerosol effects on clouds are concealed by natural cloud heterogeneity and satellite retrieval errors, Nat. Commun., 13, 7357, https://doi.org/10.1038/s41467-022-34948-5, 2022.

Beck, A., Henneberger, J., Schöpfer, S., Fugal, J., and Lohmann, U.: HoloGondel: in situ cloud observations on a cable car in the Swiss Alps using a holographic imager, Atmos. Meas. Tech., 10, 459–476, https://doi.org/10.5194/amt-10-459-2017, 2017.

Brus, D., Gustafsson, J., Vakkari, V., Kemppinen, O., de Boer, G., and Hirsikko, A.:

https://doi.org/10.5194/egusphere-2026-2088
Preprint. Discussion started: 30 June 2026

660 Measurement report: Properties of aerosol and gases in the vertical profile during the
661 LAPSE-RATE campaign, Atmospheric Chemistry and Physics, 21, 517 – 533,
662 https://doi.org/10.5194/acp-315 21-517-2021, 2021.

663 Bony, S., Stevens, B., Frierson, D. M. W., Jakob, C., Kageyama, M., Pincus, R., Shepherd,
664 T. G., Sherwood, S. C., Siebesma, A. P., Sobel, A. H., Watanabe, M., and Webb, M. J.:
665 Clouds, circulation and climate sensitivity, Nature Geoscience, 8, 261–268,
666 https://doi.org/10.1038/ngeo2398, 2015.

667 Calderón, S. M., Tonttila, J., Buchholz, A., Joutsensaari, J., Komppula, M., Leskinen, A.,
668 Hao, L., Moisseev, D., Pullinen, I., Tiitta, P., Xu, J., Virtanen, A., Kokkola, H., and
669 Romakkaniemi, S.: Aerosol–stratocumulus interactions: towards a better process
670 understanding using closures between observations and large eddy simulations, Atmos.
671 Chem. Phys., 22, 12417–12441, https://doi.org/10.5194/acp-22-12417-2022, 2022.

672 Ceppi, P. and Nowack, P.: Observational evidence that cloud feedback amplifies global
673 warming, *Proc. Natl. Acad. Sci. USA*, 118, e2026290118,
674 https://doi.org/10.1073/pnas.2026290118, 2021.

675 Cess, R. D., Potter, G. L., Blanchet, J. P., Boer, G. J., Del Genio, A. D., Déqué, M.,
676 Dymnikov, V., Galin, V., Gates, W. L., Ghan, S. J., Kiehl, J. T., Lacis, A. A., Le Treut, H., Li,
677 Z.-X., Liang, X.-Z., McAvaney, B. J., Meleshko, V. P., Mitchell, J. F. B., Morcrette, J.-J.,
678 Randall, D. A., Rikus, L., Roeckner, E., Royer, J. F., Schlese, U., Sheinin, D. A., Slingo, A.,
679 Sokolov, A. P., Taylor, K. E., Washington, W. M., Wetherald, R. T., Yagai, I., and Zhang, M.-
680 H.: Intercomparison and interpretation of climate feedback processes in 19 atmospheric
681 general circulation models, Journal of Geophysical Research: Atmospheres, 95, 16 601–
682 16 615, https://doi.org/https://doi.org/10.1029/JD095iD10p16601, 1990.

683 Chambers, T. E., Reid, I. M., and Hamilton, M.: A lightweight holographic imager for cloud
684 microphysical studies from an untethered balloon, Atmos. Meas. Tech., 17, 3237–3253,
685 https://doi.org/10.5194/amt-17-3237-2024, 2024.

686 Christensen, M. W., Jones, W. K., and Stier, P.: Aerosols enhance cloud lifetime and
687 brightness along the stratus-to-cumulus transition, *Proc. Natl. Acad. Sci. USA*, 117,
688 17591–17598, https://doi.org/10.1073/pnas.1921231117, 2020

https://doi.org/10.5194/egusphere-2026-2088
Preprint. Discussion started: 30 June 2026

689 Christensen, M. W., Wu, P., Varble, A. C., Xiao, H., and Fast, J. D.: Aerosol-induced
690 closure of marine cloud cells: enhanced effects in the presence of precipitation, Atmos.
691 Chem. Phys., 24, 6455–6476, https://doi.org/10.5194/acp-24-6455-2024, 2024.

692 Desai, N., Glienke, S., Fugal, J., and Shaw, R. A.: Search for Microphysical Signatures of
693 Stochastic Condensation in Marine Boundary Layer Clouds Using Airborne Digital
694 Holography, J. Geophys. Res.-Atmos., 124, 2739–2752,
695 https://doi.org/10.1029/2018JD029033, 2019.

696 Doulgeris, K. M., Vakkari, V., O'Connor, E. J., Kerminen, V.-M., Lihavainen, H., and Brus,
697 D.: Influence of air mass origin on microphysical properties of low-level clouds in a
698 subarctic environment, Atmos. Chem. Phys., 23, 2483–2498,
699 https://doi.org/10.5194/acp-23-2483-2023, 2023

700 Doulgeris, K. M., Kaikkonen, V., Juttula, H., Molkoselkä, E., Mäkynen, A., and Brus, D.: In
701 situ surface cloud measurement dataset from four cloud spectrometers during the
702 Pallas Cloud Experiment (PaCE) 2022, Earth Syst. Sci. Data, 17, 6497–6506,
703 https://doi.org/10.5194/essd-17-6497-2025, 2025.

704 Doulgeris, K., D. Brus, C. Maier, M. Komppula, V. Kaikkonen, H. Juttula, E. Molkoselkä, A.
705 Mäkynen, K. Julaha, N. Zikova, C. Zhang, Z. A. Kanji, S. Sel and E. Ludewig:
706 Intercomparison of Cloud Spectrometers and a Holographic Probe During the ACTRIS
707 Sub-Zero In-Cloud Campaign at Sonnblick Observatory, to be submitted to Atmos. Meas.
708 Tech., 2026.

709 Feingold, G., Goren, T., and Yamaguchi, T.: Quantifying albedo susceptibility biases in
710 shallow clouds, Atmos. Chem. Phys., 22, 3303–3319, https://doi.org/10.5194/acp-22-
711 3303-2022, 2022.

712 Fuchs, C., Ramelli, F., Schweizer, D., Lohmann, U., and Henneberger, J.: Putting the
713 spotlight on small cloud droplets with SmHOLIMO – a new holographic imager for in situ
714 measurements of clouds, Atmos. Meas. Tech., 18, 2969–2986,
715 https://doi.org/10.5194/amt-18-2969-2025, 2025.

716 Gao, R. S., H. Telg, R. J. McLaughlin, S. J. Ciciora, L. A. Watts, M. S. Richardson, J. P.
717 Schwarz, A. E. Perring, T. D. Thornberry, A. W. Rollins, M. Z. Markovic, T. S. Bates, J. E.

https://doi.org/10.5194/egusphere-2026-2088
Preprint. Discussion started: 30 June 2026

718 Johnson & D. W. Fahey (2016) A light-weight, high-sensitivity particle spectrometer for
719 PM2.5 aerosol measurements, Aerosol Science and Technology, 50:1, 88-99, DOI:
720 10.1080/02786826.2015.1131809

721 Goren, T., Choudhury, G., Kretzschmar, J., and McCoy, I.: Co-variability drives the
722 inverted-V sensitivity between liquid water path and droplet concentrations, Atmos.
723 Chem. Phys., 25, 3413–3423, https://doi.org/10.5194/acp-25-3413-2025, 2025.

724 Gryspeerdt, E., Goren, T., Sourdeval, O., Quaas, J., Mülmenstädt, J., Dipu, S., Unglaub,
725 C., Gettelman, A., and Christensen, M.: Constraining the aerosol influence on cloud
726 liquid water path, Atmos. Chem. Phys., 19, 5331–5347, https://doi.org/10.5194/acp-19-
727 5331-2019, 2019.

728 Hameri, K., Koponen, I. K., Aalto, P. P., and Kulmala, M.: The particle detection efficiency
729 of the TSI-3007 condensation particle counter, Journal of Aerosol Science, 33, 1463–
730 1469, https://doi.org/10.1016/S0021-8502(02)00090-3, 2002.

731 Hatakka, J., Aalto, T., Aaltonen, V., Aurela, M., Hakola, H., Komppula, M., Laurila, T.,
732 Lihavainen, H., Paatero, J., Salminen, K., and Viisanen, Y.: Overview of the atmospheric
733 research activities and results at Pallas GAW station, Boreal Environ. Res., 8, 365–384,
734 2003.

735 Henneberger, J., Fugal, J. P., Stetzer, O., and Lohmann, U.: HOLIMO II: a digital
736 holographic instrument for ground-based in situ observations of microphysical
737 properties of mixed-phase clouds, Atmospheric Measurement Techniques, 6, 2975–
738 2987, https://doi.org/10.5194/amt-6-2975-2013, 2013.

739 Hersbach, H., Bell, B., Berrisford, P., Biavati, G., Horányi, A., Muñoz Sabater, J., Nicolas,
740 J., Peubey, C., Radu, R., Rozum, I., Schepers, D., Simmons, A., Soci, C., Dee, D., Thépaut,
741 J-N. (2023): ERA5 hourly data on pressure levels from 1940 to present. Copernicus
742 Climate Change Service (C3S) Climate Data Store (CDS), DOI: 10.24381/cds.bd0915c6
743 (Accessed on 20-01-2025)

744 Kaikkonen, V. A., Molkoselkä, E. O., and Mäkynen, A. J.: A rotating holographic imager for
745 stationary cloud droplet and ice crystal measurements, Optical Review, 27, 205–216,
746 https://doi.org/10.1007/s10043-020-00583-y, 2020.

https://doi.org/10.5194/egusphere-2026-2088
Preprint. Discussion started: 30 June 2026

747 Kaikkonen, V. A., Molkoselkä, E. O., Juttula, H. J., and Mäkynen, A. J.: UAV cloud particle
748 sensor, IEEE International Instrumentation and Measurement Technology Conference
749 (I2MTC), Glasgow, United Kingdom, 2024, pp. 1-6,
750 https://doi.org/10.1109/I2MTC60896.2024.10560651, 2024.

751 Kainz, J., Hoffmann, F.: The effects of aerosol on small-scale cloud-environment mixing:
752 Implications for simulating and observing inhomogeneous mixing, *Journal of*
753 *Geophysical Research: Atmospheres*, 128, e2023JD038509.
754 https://doi.org/10.1029/2023JD038509, 2023.

755 Keil, A. & Wendisch, M., 2001. *Bursts of Aitken mode and ultrafine particles observed at*
756 *the top of continental boundary layer clouds*. *J. Aerosol Sci.*, 32, pp.649–660.
757 https://doi.org/10.1016/S0021-8502(00)00102-6

758 Kezoudi, M., Keleshis, C., Antoniou, P., Biskos, G., Bronz, M., Constantinides, C.,
759 Desservettaz, M., Gao, R.-S., Girdwood, J., Harnetiaux, J., Kandler, K., Leonidou, A., Liu,
760 Y., Lelieveld, J., Marenco, F., Mihalopoulos, N., Močnik, G., Neitola, K., Paris, J.-D.,
761 Pikridas, M., Sarda-Esteve, R., Stopford, Chris,Unga, F.,Vrekoussis, M. Sciare, J.: The
762 Unmanned Systems Research Laboratory (USRL): A New Facility for UAV-Based
763 Atmospheric Observations. *Atmosphere*, *12*(8), 1042.
764 https://doi.org/10.3390/atmos12081042, 2021.Kokkola, H., Tonttila, J., Calderón, S. M.,
765 Romakkaniemi, S., Lipponen, A., Peräkorpi, A., Mielonen, T., Gryspeerdt, E., Virtanen, T.
766 H., Kolmonen, P., and Arola, A.: Model analysis of biases in the satellite-diagnosed
767 aerosol effect on the cloud liquid water path, Atmos. Chem. Phys., 25, 1533–1543,
768 https://doi.org/10.5194/acp-25-1533-2025, 2025.

769 Komppula, M., Lihavainen, H., Kerminen, V.-M., Kulmala, M., and Viisanen Y.:
770 Measurements of cloud droplet activation of aerosol particles at a clean subarctic
771 background site, J. Geophys. Res., 110, D06204, https://doi.org/10.1029/2004JD005200,
772 2005.

773 Le, V., Doulgeris, K. M., Komppula, M., Backman, J., Bagheri, G., Bodenschatz, E., and
774 Brus, D.: Dataset of airborne measurements of aerosol, cloud droplets and meteorology
775 by tethered balloon during PaCE 2022, Earth Syst. Sci. Data Discuss. Submitted, 2026.

https://doi.org/10.5194/egusphere-2026-2088
Preprint. Discussion started: 30 June 2026

776 Leung, W. Y. H., J. Savre, F. A.-M. Bender, M. Komppula, H. Portin, S. Romakkaniemi, J.
777 Sedlar, K. Noone, A. M.L. Ekman: The sensitivity of a continental nighttime
778 stratocumulustopped boundary layer to varying environmental conditions, Q.J.R.
779 Meteorol. Soc.. doi:10.1002/qj.2877, 2016.

780 Lohila, A., Penttilä, T., Jortikka, S., Aalto, T., Anttila, P., Asmi, E., Aurela, M., Hatakka, J.,
781 Hellén, H., Henttonen, H., Hänninen, P., Kilkki, J., Kyllönen, K., Laurila, T., Lepistö, A.,
782 Lihavainen, H., Makkonen, U., Paatero, J., Rask, M., Sutinen, R., Tuovinen, J.-P.,
783 Vuorenmaa, J., and Viisanen, Y.: Preface to the special issue on integrated research of
784 atmosphere, ecosystems and environment at Pallas, Boreal Environ. Res., 20, 431–454,
785 2015.

786 Molkoselkä, E. O., Kaikkonen, V. A., and Mäkynen, A. J.: Measuring Atmospheric Icing
787 Rate in Mixed-Phase Clouds Using Filtered Particle Data, IEEE Transactions on
788 Instrumentation and Measurement, 70, 1–8, https://doi.org/10.1109/TIM.2020.3035562,
789 2021.O'Connor, E.: Classification data from Kenttärova on 13 September 2023, ACTRIS
790 Cloud remote sensing data centre unit (CLU),
791 https://hdl.handle.net/21.12132/1.25e5346012244ce4, 2024a.

792 O'Connor, E.: Classification data from Kenttärova on 27 September 2023, ACTRIS Cloud
793 remote sensing data centre unit (CLU),
794 https://hdl.handle.net/21.12132/1.eed816412e95425b, 2024b.

795 O'Connor, E.: Classification data from Kenttärova on 29 September 2023, ACTRIS Cloud
796 remote sensing data centre unit (CLU),
797 https://hdl.handle.net/21.12132/1.a94a56eb247b4535, 2024c.

798 Pilz, C., Düsing, S., Wehner, B., Müller, T., Siebert, H., Voigtländer, J., and Lonardi, M.:
799 CAMP: an instrumented platform for balloon-borne aerosol particle studies in the lower
800 atmosphere, Atmospheric Measurement Techniques, 15, 6889–6905,
801 https://doi.org/10.5194/amt-15-6889-2022, 2022.

802 Pohorsky, R., Baccarini, A., Tolu, J., Winkel, L. H. E., and Schmale, J.: Modular
803 Multiplatform Compatible Air Measurement System (MoMuCAMS): a new modular
804 platform for boundary layer aerosol and trace gas vertical measurements in extreme

https://doi.org/10.5194/egusphere-2026-2088
Preprint. Discussion started: 30 June 2026

environments, Atmospheric Measurement Techniques, 17, 731–754, https://doi.org/10.5194/amt-17-731-2024, 2024.

Possner, A., Eastman, R., Bender, F., and Glassmeier, F.: Deconvolution of boundary layer depth and aerosol constraints on cloud water path in subtropical stratocumulus decks, Atmos. Chem. Phys., 20, 3609–3621, https://doi.org/10.5194/acp-20-3609-2020, 2020.

Romakkaniemi, S., Maalick, Z., Hellsten, A., Ruuskanen, A., Väisänen, O., Ahmad, I., Tonttila, J., Mikkonen, S., Komppula, M., and Kühn, T.: Aerosol–landscape–cloud interaction: signatures of topography effect on cloud droplet formation, Atmos. Chem. Phys., 17, 7955–7964, https://doi.org/10.5194/acp-17-7955-2017, 2017.

Schlenczek, O., Nordsiek, F., Brunner, C. E., Chávez-Medina, V., Thiede, B., Bodenschatz, E., and Bagheri, G.: Airborne measurements of turbulence and cloud microphysics during PaCE 2022 using the Advanced Max Planck CloudKite Instrument (MPCK⁺), Earth Syst. Sci. Data Discuss. [preprint], https://doi.org/10.5194/essd-2025-112, in review, 2025.

Stephens, G. L.: Cloud feedbacks in the climate system: A critical review, Journal of Climate, 18, 237 – 273, https://doi.org/https://doi.org/10.1175/JCLI-3243.1, 2005.

Stevens, B., Moeng, C.-H., Ackerman, A. S., Bretherton, C. S., Chlond, A., de Roode, S., Edwards, J., Golaz, J.-C., Jiang, H., Khairoutdinov, M., Kirkpatrick, M. P., Lewellen, D. C., Lock, A., Müller, F., Stevens, D. E., Whelan, E., and Zhu, P.: Evaluation of large-eddy simulations via observations of nocturnal marine stratocumulus, *Mon. Weather Rev.*, 133, 1443–1462, https://doi.org/10.1175/MWR2930.1, 2005

Stevens, B., and Feingold, G.: Untangling aerosol effects on clouds and precipitation in a buffered system, Nature, 461, 607–613, https://doi.org/10.1038/nature08281, 2009.

Tiitta, P., Leskinen, A., Kaikkonen, V. A., Molkoselkä, E. O., Mäkynen, A. J., Joutsensaari, J., Calderón, S., Romakkaniemi, S., and Komppula, M.: Intercomparison of holographic imaging and single-particle forward light scattering in situ measurements of liquid clouds in changing atmospheric conditions, Atmospheric Measurement Techniques, 15, 2993–3009, https://doi.org/10.5194/amt-15-2993-2022, 2022.

https://doi.org/10.5194/egusphere-2026-2088
Preprint. Discussion started: 30 June 2026

Tonttila, J., Maalick, Z., Raatikainen, T., Kokkola, H., Kühn, T., and Romakkaniemi, S.: UCLALES–SALSA v1.0: a large-eddy model with interactive sectional microphysics for aerosol, clouds and precipitation, Geosci. Model Dev., 10, 169–188, https://doi.org/10.5194/gmd-10-169-2017, 2017.

Tonttila, J., Afzalifar, A., Kokkola, H., Raatikainen, T., Korhonen, H., and Romakkaniemi, S.: Precipitation enhancement in stratocumulus clouds through airborne seeding: sensitivity analysis by UCLALES-SALSA, Atmos. Chem. Phys., 21, 1035–1048, https://doi.org/10.5194/acp-21-1035-2021, 2021.

Tukiainen, S., Siipola, T., Leskinen, N., and O'Connor, E.: Remote sensing measurements during PaCE 2022 campaign, Earth Syst. Sci. Data, 17, 3797–3806, https://doi.org/10.5194/essd-17-3797-2025, 2025.

Twomey, S. A.: The influence of pollution on the shortwave albedo of clouds, J. Atmos. Sci., 34, 1149–1152, https://doi.org/10.1175/1520-0469(1977)034<1149:TIOPOT>2.0.CO;2, 1977.

Virtanen A., J. Joutsensaari, H. Kokkola, D. Partridge, S. M. Blichner, Ø. Seland, E. Holopainen, E. Tovazzi, A. Lipponen, S. Mikkonen, A. Leskinen , A. Hyvärinen, P. Zieger, Dr Radovan Krejci, A. Ekman, I. Riipinen, J. Quaas, and S. Romakkaniemi: High sensitivity of cloud formation to aerosol changes. Nat. Geosci. https://doi.org/10.1038/s41561-025-01662-y, 2025

Wiedensohler, A., Wiesner, A., Weinhold, K., Birmili, W., Hermann, M., Merkel, M., Muller, T., Pfeifer, S., Schmidt, A., Tuch, T., Velarde, F., Quincey, P., Seeger, S., and Nowak, A.: Mobility particle size spectrometers: Calibration procedures and measurement uncertainties, Aerosol Science and Technology, 52, 146–164, https://doi.org/10.1080/02786826.2017.1387229, 2018.

Yeom, J.M., Fahandezh Sadi, H., Anderson, J.C., Yang F., Cantrell W., and Shaw R.: Cloud microphysical response to entrainment of dry air containing aerosols. *npj Clim Atmos Sci* **8**, 8, https://doi.org/10.1038/s41612-024-00889-7, 2025.

Zhang, C., Wang, J., Yang, C., Zhou, H., Liu, J., and Hua, D.: A Comparative Investigation of Light Scattering and Digital Holographic Imaging to Measure Liquid Phase Cloud

https://doi.org/10.5194/egusphere-2026-2088
Preprint. Discussion started: 30 June 2026

863 Droplets, Atmosphere, 14, https://doi.org/10.3390/atmos14091381, 2023.

864

https://doi.org/10.5194/egusphere-2026-2088
Preprint. Discussion started: 30 June 2026

865 FIGURES AND TABLES

866

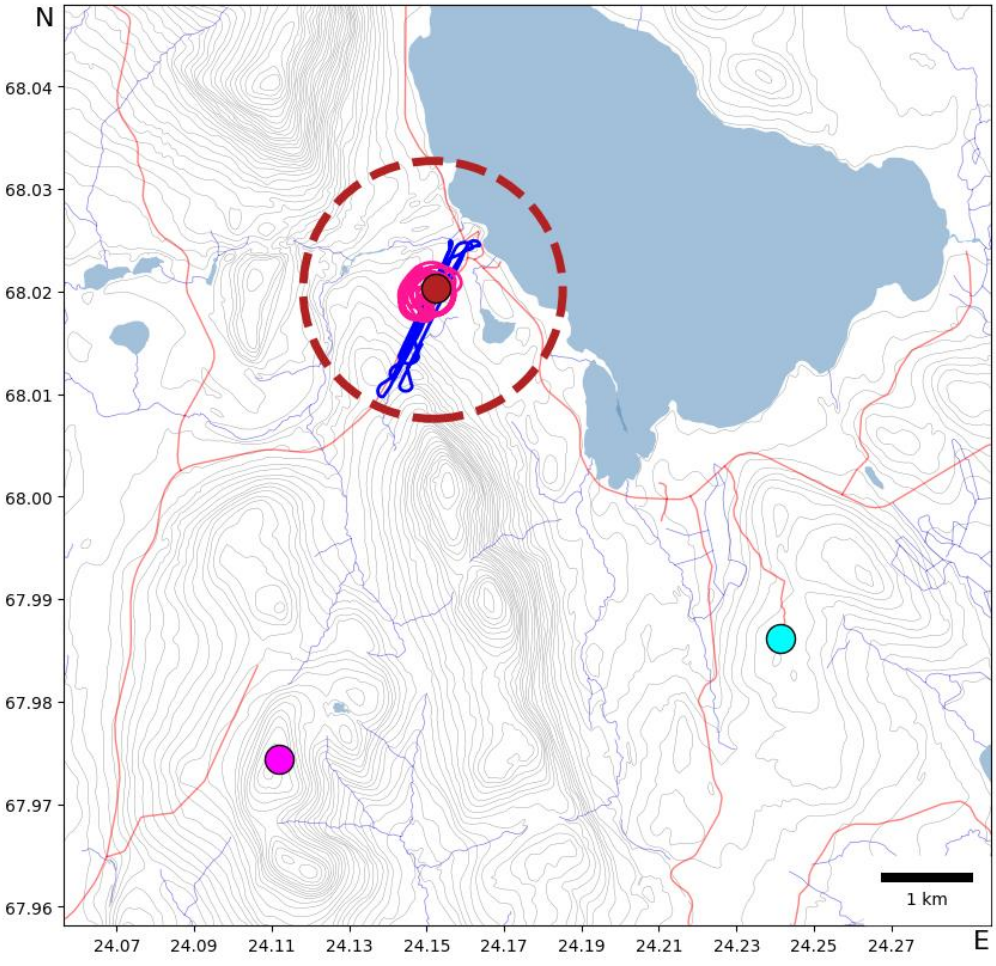

867

868 Figure 1. Map of Pallas campaign site. Red dot = UAV launch field, magenta dot =
869 Sammaltunturi station (ICEMET, aerosols, meteorology), cyan dot = Kenttärova station
870 (Cloudnet). The distance among places is approx. 5 km, red circle = the maximum range
871 of the flights, blue line = path of flight T2, pink line = path of flight V4. The map contains
872 open data from the National Land Survey of Finland Topographic Database 03/2024
873 (under CC 4.0 license).

https://doi.org/10.5194/egusphere-2026-2088
Preprint. Discussion started: 30 June 2026

Figure 2. The UAV-CPS mounted on the nose of the Talon UAV.

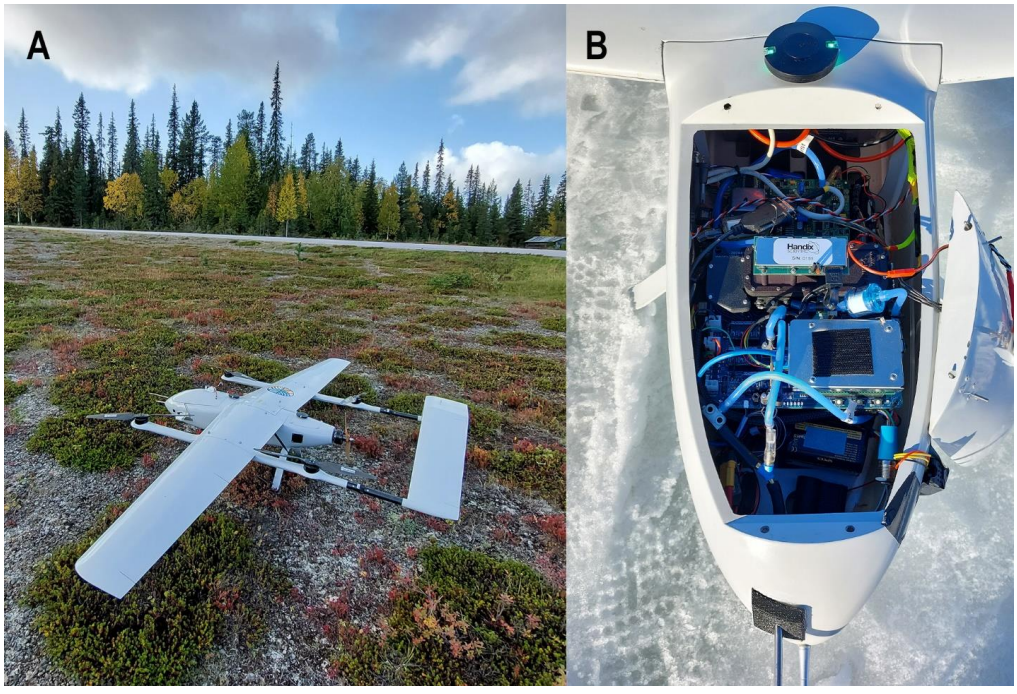

Figure 3: The vertical take-off and landing (VTOL) uncrewed aircraft system (UAS) platform, callsign Marta (A) and its inner volume for scientific instruments (B).

https://doi.org/10.5194/egusphere-2026-2088
Preprint. Discussion started: 30 June 2026

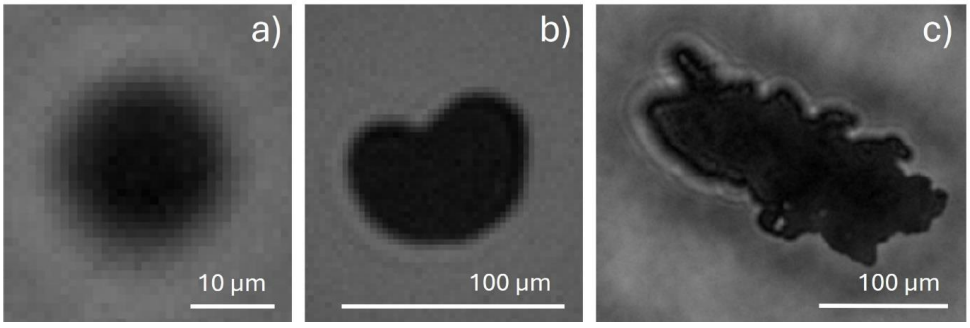

Figure 4. Examples of particle shadow images captured by the UAV-CPS instrument. a) cloud droplet, b) pine pollen and c) ice crystal. Equivalent diameters of particles are 20 µm, 71 µm and 286 µm, respectively.

https://doi.org/10.5194/egusphere-2026-2088
Preprint. Discussion started: 30 June 2026

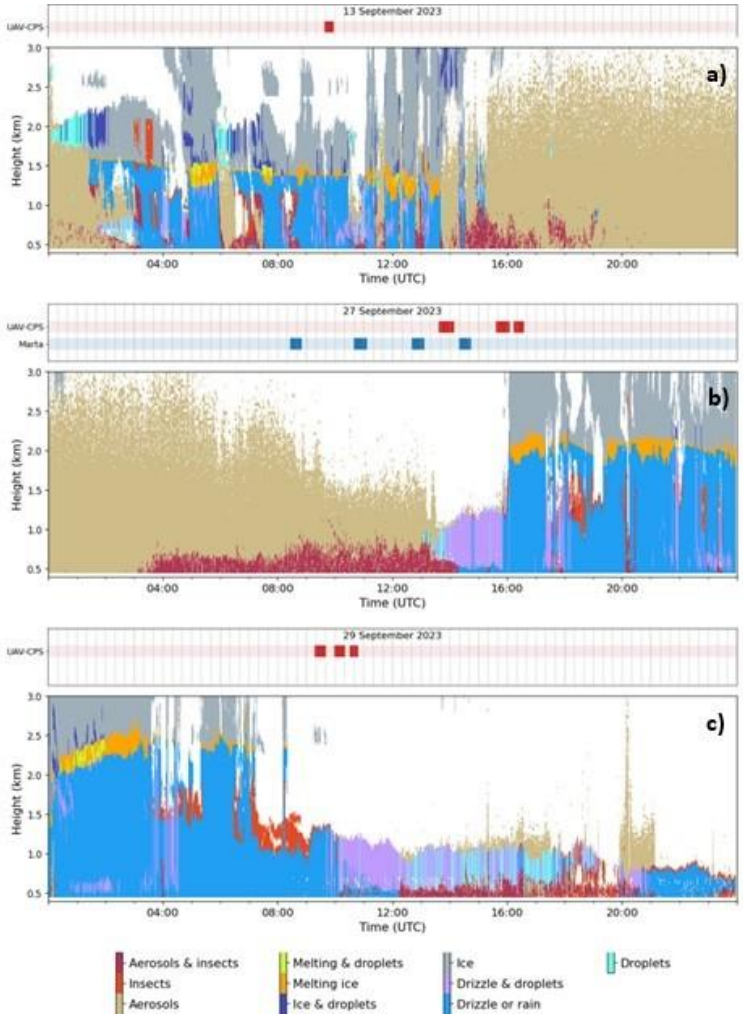

Figure 5. The times of the flights with UAV-CPS and Aerosol-VTOL (callsign Marta) are shown along with the Cloudnet target classification, zoomed to 0.4–3 km, of the respective day. Three different days were investigated: (a) 13, (b) 27, and (c) 29 September 2023.

https://doi.org/10.5194/egusphere-2026-2088
Preprint. Discussion started: 30 June 2026

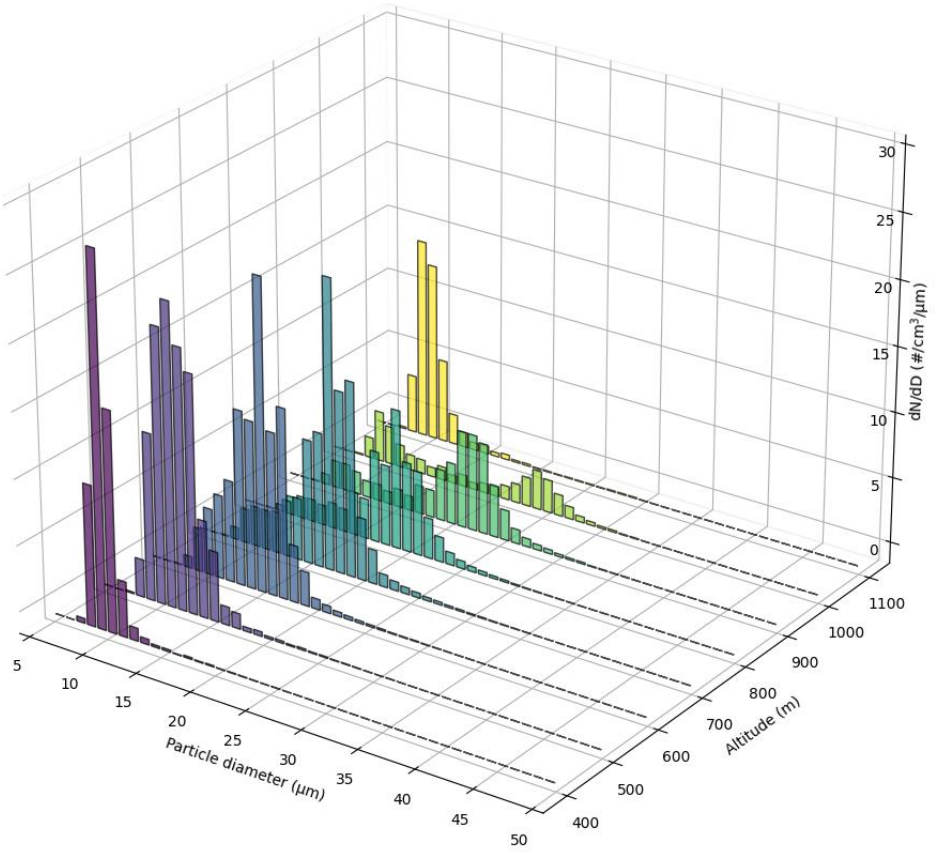

Figure 6. Particle size distributions measured with UAV-CPS at 400–1200 m height during flight T4. The size distributions are averaged over 100 m altitude bins.

https://doi.org/10.5194/egusphere-2026-2088
Preprint. Discussion started: 30 June 2026

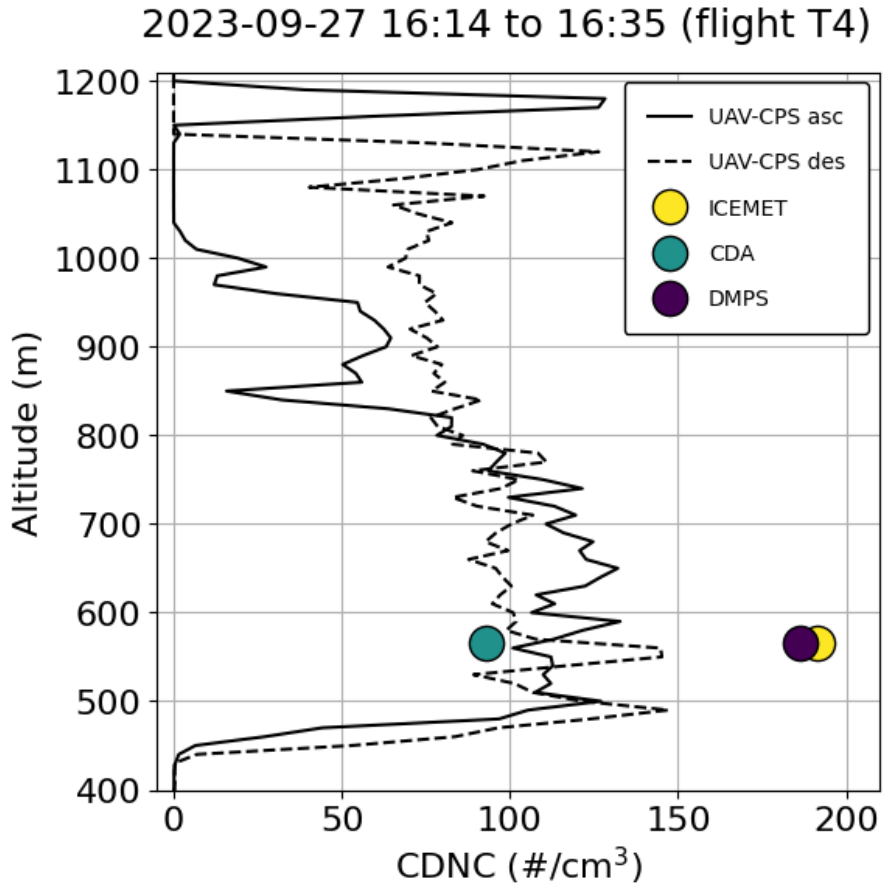

Figure 7. The cloud droplet number concentration (CDNC) during flight T4, measured with UAV-CPS (black) during ascent (solid line) and descent (dashed line), ICEMET (bright yellow), and CDA (dark cyan), and that estimated from the DMPS analysis (dark purple).

https://doi.org/10.5194/egusphere-2026-2088
Preprint. Discussion started: 30 June 2026

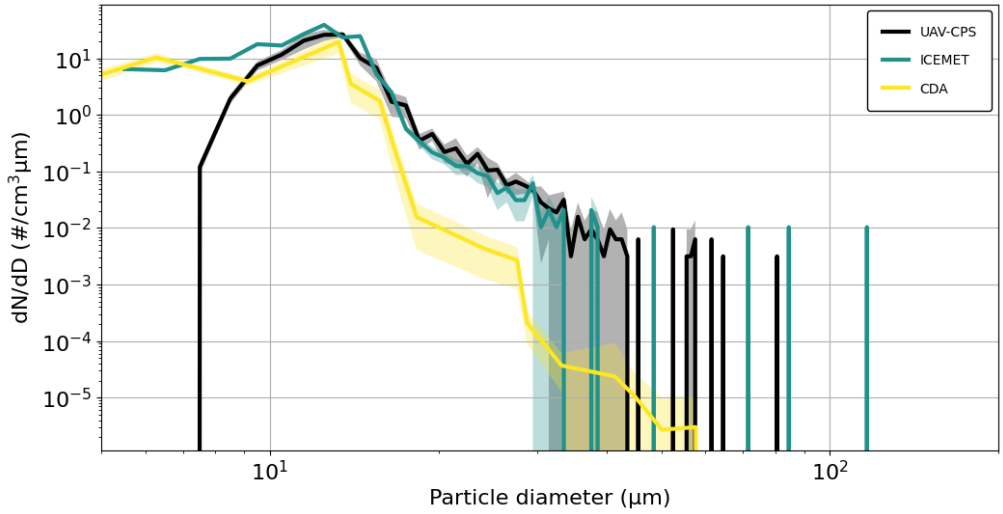

Figure 8. The average particle size distribution measured with UAV-CPS when at 550–580 m altitude, and those measured with ICEMET and CDA at Sammaltunturi during flight T4. The shaded areas are standard deviations and indicate the extent of variation.

https://doi.org/10.5194/egusphere-2026-2088
Preprint. Discussion started: 30 June 2026

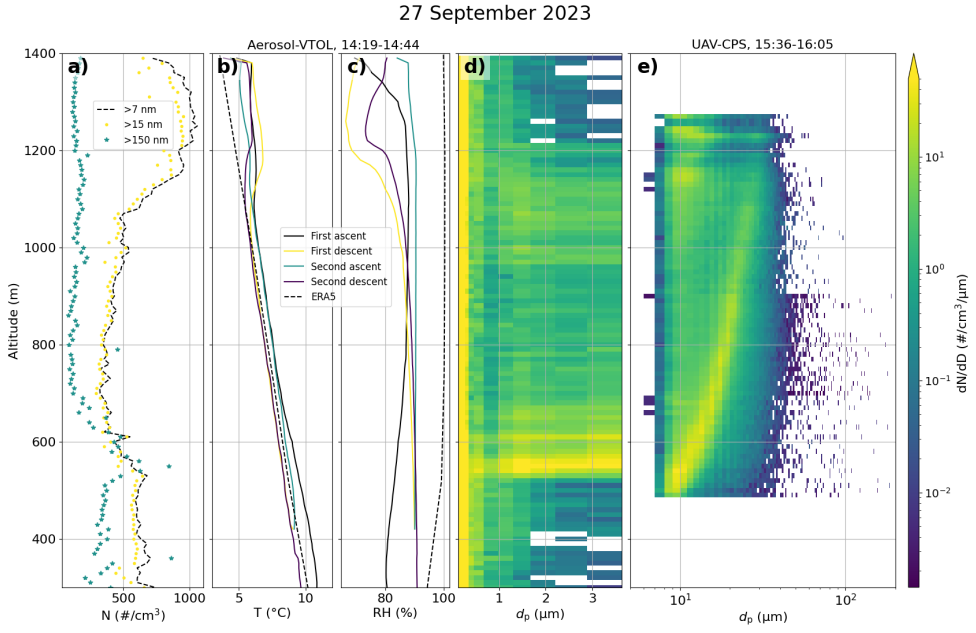

Figure 9. Vertical profiles of: a) number concentration (N) for particles >7 nm, >15 nm, and >150 nm, b) temperature (T), c) relative humidity (RH), and d) & e) size distribution of particles >150 nm, combined from flights V4 and T3. Temperature and relative humidity are shown separately for each ascent and descent, while all other curves represent averages over the entire flight.

https://doi.org/10.5194/egusphere-2026-2088
Preprint. Discussion started: 30 June 2026

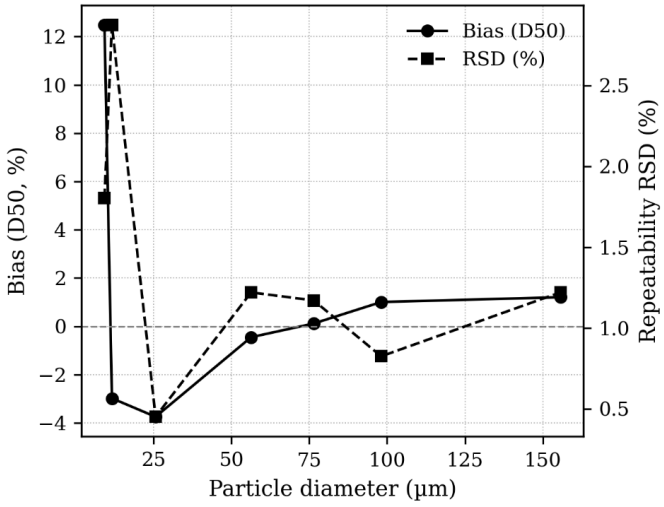

Figure 10. For D50, size-dependent bias (left axis) and repeatability presented as relative standard deviation (RSD, right axis) from the calibration bead measurements. The results indicate that while the repeatability remains low (under 3%), systematic bias is clearly larger for the smallest particles. This highlights the influence of optical resolving power limit on sizing accuracy.

https://doi.org/10.5194/egusphere-2026-2088
Preprint. Discussion started: 30 June 2026

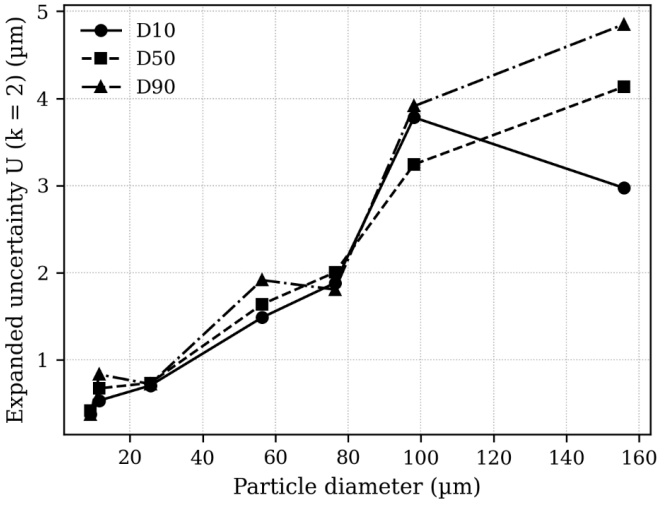

942

943

944 Figure 11. Combined expanded uncertainty (k=2) for D10, D50 and D90 as a function of
945 particle diameter. The results show the size-dependent uncertainty across different
946 parts of the particle size distribution (PSD), the variations reflect both measurement
947 repeatability and reference glass bead size uncertainty.

948

https://doi.org/10.5194/egusphere-2026-2088
Preprint. Discussion started: 30 June 2026

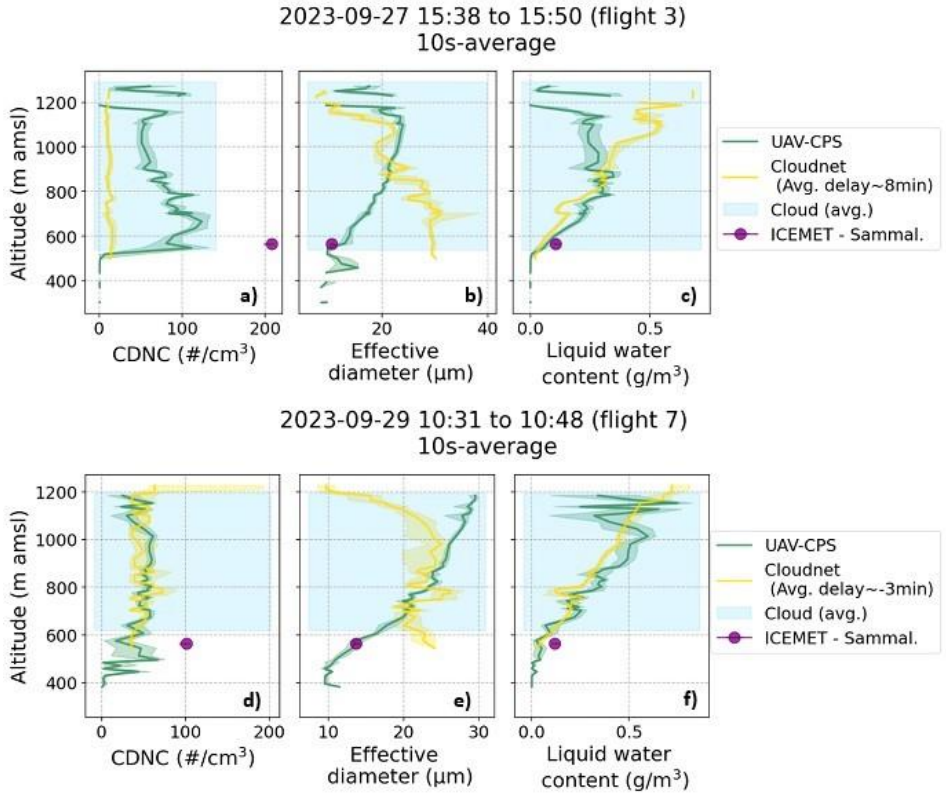

Figure 12. Vertical profiles of cloud droplet number concentration (a & d), effective diameter (b & e), and liquid water content (c & f)) calculated from the UAV-CPS data from Cloudnet and Sammaltunturi station measurements. The observations are matched by using mean wind and corresponding delays, 8 min for 27 September 2023 (a-c) and 3 min for 29 September 2023 (d-f). The blue shading depicts cloud boundaries as determined by Cloudnet.

https://doi.org/10.5194/egusphere-2026-2088
Preprint. Discussion started: 30 June 2026

964 Table 1. Flights with UAV-CPS mounted on Talon UAV.

Flight	Start time (UTC)	End time (UTC)	Maximum altitude (m)	Cloud top (m)
T1	2023-09-13 09:37	2023-09-13 09:57	2290	1290
T2	2023-09-27 13:37	2023-09-27 14:09	1610	890
T3	2023-09-27 15:36	2023-09-27 16:05	1300	1270
T4	2023-09-27 16:14	2023-09-27 16:35	1550	1190
T5	2023-09-29 09:17	2023-09-29 09:41	1900	1330
T6	2023-09-29 09:58	2023-09-29 10:21	1600	1170
T7	2023-09-29 10:31	2023-09-29 10:48	1760	1170

965

966 Table 2. Flights with POPS and CPCs mounted on VTOL.

Flight	Start time (UTC)	End time (UTC)	Maximum altitude (m)
V1	2023-09-27 08:26	2023-09-27 08:50	1200
V2	2023-09-27 10:39	2023-09-27 11:06	1290
V3	2023-09-27 12:41	2023-09-27 13:07	1900
V4	2023-09-27 14:19	2023-09-27 14:44	1900

967